PNAS RESEARCH ARTICLE | BIOPHYSICS AND COMPUTATIONAL BIOLOGY
ENVIRONMENTAL SCIENCES OPEN ACCESS

Spatially explicit effective reproduction numbers from incidence and mobility data

Cristiano Trevisin[a], Enrico Bertuzzo[b], Damiano Pasetto[b], Lorenzo Mari[c], Stefano Miccoli[d], Renato Casagrandi[c], Marino Gatto[c], and Andrea Rinaldo[a,e,1]

Contributed by Andrea Rinaldo; received November 20, 2022; accepted March 28, 2023; reviewed by Stefano Merler and Alessandro Vespignani

Current methods for near real-time estimation of effective reproduction numbers from surveillance data overlook mobility fluxes of infectors and susceptible individuals within a spatially connected network (the metapopulation). Exchanges of infections among different communities may thus be misrepresented unless explicitly measured and accounted for in the renewal equations. Here, we first derive the equations that include spatially explicit effective reproduction numbers, $\mathcal{R}_k(t)$, in an arbitrary community k. These equations embed a suitable connection matrix blending mobility among connected communities and mobility-related containment measures. Then, we propose a tool to estimate, in a Bayesian framework involving particle filtering, the values of $\mathcal{R}_k(t)$ maximizing a suitable likelihood function reproducing observed patterns of infections in space and time. We validate our tools against synthetic data and apply them to real COVID-19 epidemiological records in a severely affected and carefully monitored Italian region. Differences arising between connected and disconnected reproduction numbers (the latter being calculated with existing methods, to which our formulation reduces by setting mobility to zero) suggest that current standards may be improved in their estimation of disease transmission over time.

infection spreading mechanisms | human mobility | disease generation interval | particle filtering | COVID-19

Significance

The effective reproduction number quantifies the average number of secondary infections caused by an infected individual (within the population of their own resident community, or anywhere else) when the pool of susceptibles, the epidemiological conditions, and the related control measures may change in time. Estimates of the effective reproduction number from spatial data are essential in assessing public health policies and in communication about the state of an unfolding epidemic. Statistically robust estimates of reproduction numbers from surveillance data exist, quantifying temporal changes in disease transmission. However, what is missing to date is a set of space-explicit renewal equations that quantify infections imported to (and exported from) each community. Including spatial connections would imply a more accurate description of transmission mechanisms.

The effective reproduction number of a community k at time t, $\mathcal{R}_k(t)$, defines the expected number of secondary infections caused by a single infector residing in a nonnaive community k. It is adopted to measure the level of transmission when the pool of susceptibles may have changed from its disease-free equilibrium value or transmission dynamics of the infectious disease may have shifted, owing to variations in viral transmissibility or to the effects of containment interventions (1–5). With reference to COVID-19 epidemic spread, values of $\mathcal{R}_k(t)$ are currently estimated from cohort studies (4–10) or epidemiological models (11–17). $\mathcal{R}_k(t)$ of COVID-19 has been used extensively to monitor and predict near real-time changes in transmission by mechanistic models of disease dynamics, possibly spatially explicit and individual based (12–16, 18, 19).

Direct estimates of $\mathcal{R}_k(t)$ from epidemiological data (8, 14, 19–22) are variably endowed with statistical insight and accuracy (9). However, existing methods are known to provide robust estimates of $\mathcal{R}_k(t)$ incorporating uncertainties in the distribution of serial and generation intervals, latency, and notifications of death and recovery/discharge (7, 9, 10, 17, 22, 23). When observational data are collected over a limited period of time, and several parameters need to be estimated, sources of bias abound (7). Limits to the reliability of stochastic methods have been carefully verified in particular for the recommended (9) standard computational method (8). The latter is shown to lose meaning for the k-th community when the newly reported cases reduce below a critical threshold, thus setting a practical limit to the possible spatial granularity of the analyses. Over time, $\mathcal{R}_k(t)$ detects changes in disease transmission within the k-th community. Although less prognostic than the reactivity of the system to the seeding of new infections (19), its immediacy (say, its possible exceedance of the unit value threshold) makes it universally understandable—and used. During the COVID-19 pandemic, $\mathcal{R}_k(t)$ thus became the standard indicator of the effects of epidemiological interventions and of how changes in containment policies, population immunity, and other factors affect disease transmission.

Results

We introduce a rigorous spatial extension of an integro-differential Lotka-like approach to COVID-19 modeling (*Materials and Methods* and *SI Appendix*). We consider a

Author contributions: C.T., E.B., D.P., M.G., and A.R. designed research; C.T., E.B., D.P., L.M., M.G., and A.R. performed research; C.T., E.B., D.P., L.M., S.M., R.C., M.G., and A.R. analyzed data; and C.T., L.M., S.M., R.C., M.G., and A.R. wrote the paper.

Reviewers: S.M., Fondazione Bruno Kessler; and A.V., Northeastern University.

The authors declare no competing interest.

[1]To whom correspondence may be addressed. Email: andrea.rinaldo@epfl.ch.

This article contains supporting information online at http://www.pnas.org/lookup/suppl/doi:10.1073/pnas.2219816120/-/DCSupplemental.

Published May 9, 2023.

metapopulation composed of N communities connected by human mobility where the incidence of infected individuals is suitably monitored in time by recording the number of (reported) new infections at time t and location l ($l = 1, \ldots, N$). Specifically, we consider the case of individuals resident in community l infecting or getting infected in the same community or, being mobile, in another connected site. Thus, our estimation of $\mathcal{R}_l(t)$ allows us to evaluate how mobility may contribute to the epidemic spread within a metapopulation. A key distinction is made, however, between estimates of the time evolution of local reproduction numbers $\mathcal{R}_l^{\mathrm{c}}(t)$ in each of the N communities when mobility is accounted for and the standard method that estimates the disconnected reproduction number, $\mathcal{R}_l^{\mathrm{d}}(t)$. In the latter case, the effective reproduction number is estimated by neglecting secondary infections produced via contacts with residents outside l (8, 9), thus assuming that all infections are generated in situ by the disease demography. Obviously, when internally generated infections are dominant in a given geographic context, one expects $\mathcal{R}_l^{\mathrm{c}}(t) \simeq \mathcal{R}_l^{\mathrm{d}}(t)$. The effective reproduction number $\mathcal{R}_l^{\mathrm{c}}(t)$ of the l-th community accounts for the secondary infections produced by a resident of l either in the same community l or elsewhere in any other connected one, assuming that the residents retain the same number even when they produce infections in a foreign node. Alternative formulations entailing a different meaning of $\mathcal{R}_l^{\mathrm{c}}(t)$ may be adopted to account for different roles of, and reflecting different transmission routes for, foreign infections (*SI Appendix*, section 3). Our main methodological result (*Materials and Methods*) is an integral equation producing an estimate $\hat{F}_l(t)$ of the incidence of the new cases in node l at time t. It involves the connected reproduction numbers, $\mathcal{R}_k^{\mathrm{c}}(t)$, and a stochastic connection matrix, $C_{jl}(t)$, quantifying the probability that one susceptible/infected individual resident in l is found at location j at time t (possibly with $j = l$), i.e.,

$$\hat{F}_l(t) = \sum_{j=1}^{N} p_{jl}(t) \sum_{k=1}^{N} C_{jk}(t)\mathcal{R}_k^{\mathrm{c}}(t) \int_0^{\infty} \beta(\tau) F_k(t-\tau)\mathrm{d}\tau, \quad [1]$$

where $p_{jl}(t)$ is the fraction of residents of l temporarily present in node j, $p_{jl}(t) = C_{jl}(t)n_l / [\sum_{m=1}^{N} C_{jm}(t)n_m]$; n_l is the number of residents in node l; $F_l(t)$ is the incidence of reported new cases in node l at time t; and $\beta(t)$ defines the probability distribution function of the disease generation times, i.e., the time elapsed between an infector's contagion and that of their infectees, treated as a random variable (*Materials and Methods*). Standard estimates of the disconnected effective reproduction number $\mathcal{R}_l^{\mathrm{d}}(t)$ are obtained by setting the connection matrix $\mathbf{C} = \mathbf{I}$, thus yielding

$$\hat{F}_l(t) = \mathcal{R}_l^{\mathrm{d}}(t) \int_0^{\infty} \beta(\tau) F_l(t-\tau)\mathrm{d}\tau. \quad [2]$$

To compute the connected and disconnected effective reproduction numbers, we solve Eqs. **1** and **2**, respectively, in a sequential Monte Carlo framework (SMC, or particle filtering) (24–27) to estimate from epidemiological and mobility data the various reproduction numbers that best explain the monitored incidence. To estimate the effective reproduction numbers, we employ normalized incidences $I_k(t) = F_k(t)/n_k$ which require a lognormal likelihood instead of the classical Poisson one (*Materials and Methods* and *SI Appendix*). We thus estimate directly the external drivers of infections in any node l (i.e., the seeding of new cases in time) generated by, or induced on, nonresidents in l through contacts made possible by human mobility and by the lack of personal protection. Imported infections may originate outbreaks within naive populations and force disease dynamics through evolving avenues for susceptible-infected contacts. Spreading of infections is therefore studied in a more general manner than implied by current standards, however still being estimated directly from incidence data.

The first test application of our approach uses a synthetic dataset generated on an interconnected three-node network (Fig. 1*D*), explicitly constructed by assigning fictitious timeseries of reproduction numbers $\mathcal{R}_l^{\mathrm{true}}(t)$ to each node (Fig. 1*A*). Incidences are then generated by using the fictitious $\mathcal{R}_l^{\mathrm{true}}(t)$ and a connection matrix $\mathbf{C}$ in Eq. **1** (Fig. 1*B*). In this case, $\mathbf{C}$ is constructed by assigning the outgoing probability $\xi_l(t)$ for each node l (Fig. 1*E*) and the relative fraction of $\xi_l(t)$ that reaches each connected node (Fig. 1*D*, Section D of *Materials and Methods*). The filtering procedure is then applied to the generated epidemiological data to provide an estimate of the original $\mathcal{R}_l^{\mathrm{true}}(t)$.

The purpose of the first example, based on imposed effective reproduction numbers (Fig. 1*A*) and on given connections and time-varying mobility (Fig. 1 *D* and *E*), is to prove the accuracy

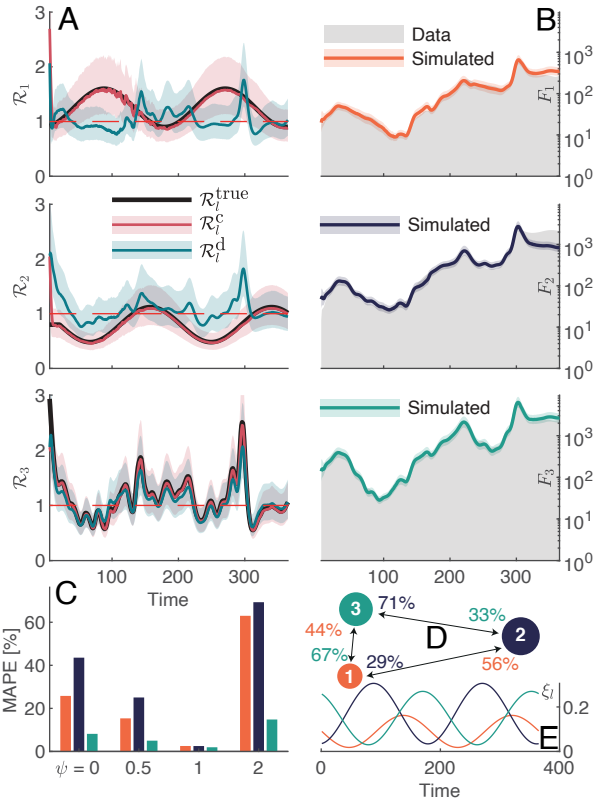

Fig. 1. Application of the SMC approach to a fictitious network of three nodes (of n_1 = 80,000, n_2 = 450,000, and n_3 =700,000 residents). (*A*) Temporal evolution of the effective reproduction numbers assigned to each node (true: $\mathcal{R}_l^{\mathrm{true}}$, estimated connected: $\mathcal{R}_l^{\mathrm{c}}$, and estimated disconnected: $\mathcal{R}_l^{\mathrm{d}}$). (*B*) daily number of infections in each node generated by using Eq. **1** with $\mathcal{R}_l^{\mathrm{true}}$ (grey shaded area), and the estimated $\mathcal{R}_l^{\mathrm{c}}$ (solid lines for median and shaded ribbons for 90% confidence interval, C.I.); (*C*) Mean absolute percentage error (MAPE) between $\mathcal{R}_l^{\mathrm{true}}$ and the estimates obtained using the disconnected approach ($\psi = 0$), the connected approach with the correct mobility ($\psi = 1$), and lower or higher outgoing mobility ($\psi = 0.5$ or 2, respectively, Section B of the *Materials and Methods*); (*D*) Three-node network and its assigned baseline relative fractions of the outgoing mobility that reach the other nodes; (*E*) Assigned outgoing mobility and its temporal variations.

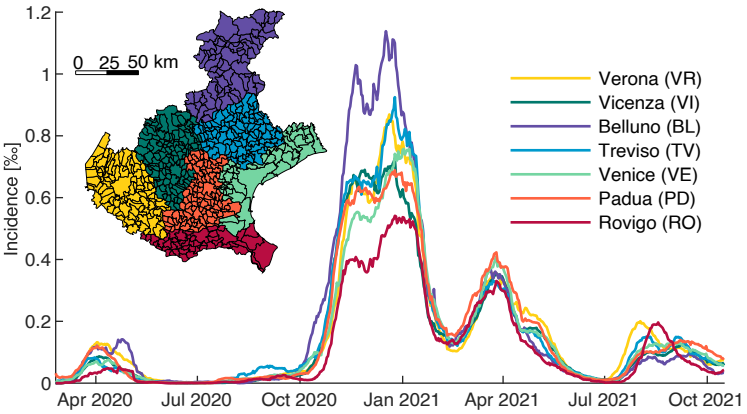

Fig. 2. Time evolution of COVID-19 monitored incidence of new positive tests (curated data from reported infections) in the seven provinces of Region Veneto (IT). A detailed map of the region highlighting the smallest possible administrative subdivision (the municipalities) is shown together with the color code identifying each province. The spatial granularity chosen for the application of the method proposed in this paper is based on the applicability of the method in the given epidemiological context, i.e., the lower limit of the number of new cases reported (8). In the case at hand, many municipalities would be often below the limit, whereas provinces (color-coded here), on average aggregating dozens of municipalities, would not. However, the tools may be adapted to any spatial arrangement of connected communities depending on the recorded attack rates and on the computational power available.

of the proposed tools in retrieving the correct values of $R_l(t)$ and to highlight the importance of including the mobility in the estimation process. We find that the spatially explicit estimates $\mathcal{R}_l^{\mathrm{c}}(t)$ of the known values $\mathcal{R}_l^{\mathrm{true}}(t)$, obtained using the SMC method and the correct connectivity, accurately reproduce the imposed values in each node (Fig. 1 *A* and *B*). On the contrary, if we had used the traditional disconnected values $\mathcal{R}_l^{\mathrm{d}}(t)$ that ignore the effects of mobility, both the trends and the absolute values of the true reproduction numbers would have been significantly under or overestimated in nodes 1 and 2 (Fig. 1*A*). However, our method is predicated on mobility being known with sufficient accuracy. The errors on the estimate grow substantially with the importance of the miscalculation of mobility (Fig 1*C*), here epitomized by a dimensionless multiplier, ψ, of the fraction of mobile individuals. Estimates prove less precise also during lull phases of the epidemic, in line with current methods (8). In any case, the relevance of the accounting for spatial effects in this example is clear. The test example thus shows that, under specific feasible conditions, $\mathcal{R}_l^{\mathrm{c}}(t) \neq \mathcal{R}_l^{\mathrm{d}}(t)$ and that the computational procedure set up to solve Eq. **1** is sound.

The second example refers to the recorded COVID-19 cases in Region Veneto in Northern Italy (Fig. 2), home to 4.9 10^6 residents and severely affected by the pandemic. Whenever one deals with real data, the problem arises of how to account for measured incidence (the data) as compared to real incidence (our model). The filtering procedure proposed in the previous example is appropriate if the proportion of real incidence identified via swab testing is fairly homogeneous in space and time (thus, possible heterogeneities, e.g., due to laboratories' capacity, healthcare policies, and general willingness to get tested, are neglected). In this sense, Region Veneto is quite appropriate because in Italy, the health system is organized at the regional level and throughout the pandemic, Veneto has adopted a strong policy of large-scale swab testing (as of October 2021, a total of 2.59 tests/resident have been carried out in this Region, as opposed to a much lower country-wide value of 1.64 tests/resident, https://github.com/pcm-dpc/COVID-19). The epidemiological timeseries studied here are shown in Fig. 2 and are limited until October 2021. This is directly linked to our assumptions (*Materials and Methods*): As the Omicron variant of SARS-CoV-2 began its ascent at the end of 2021, questions arise on whether the distribution of generation times, expressed by variable β in Eq. **1**, should have been modified had we decided to extend the computations further (but refs. 28 and 29). To estimate mobility between communities, we combined various sources, including mobile phone tracking data (*Materials and Methods*).

The results shown in Fig. 3 confirm that estimates of disconnected effective reproduction numbers from epidemiological data alone may misrepresent changes in disease transmission over time when mobility involves a significant fraction of the

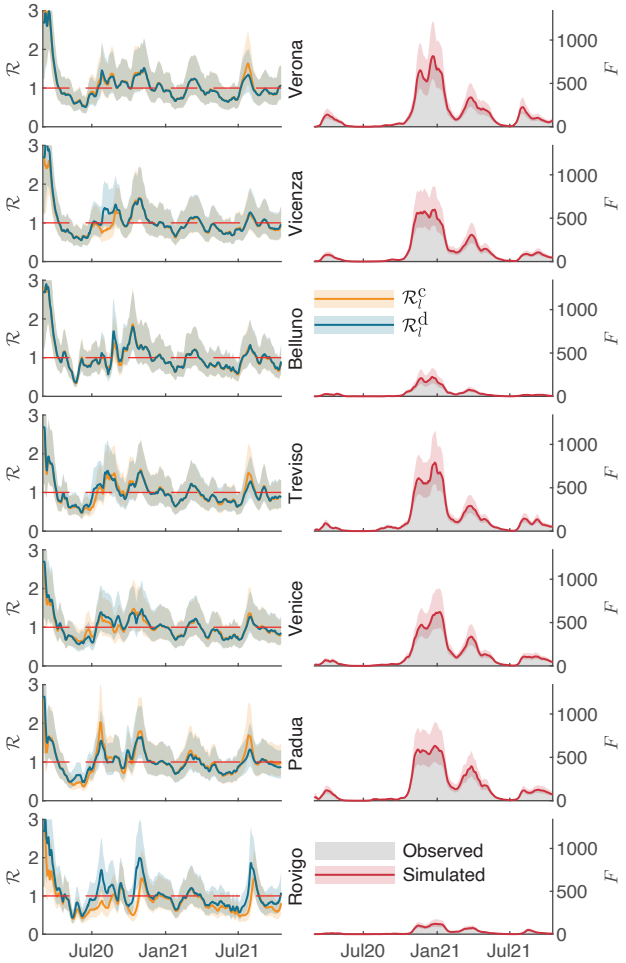

Fig. 3. Differences arising in the estimation of the effective reproduction numbers when human mobility is accounted ($\mathcal{R}_l^{\mathrm{c}}$, in orange) or not ($\mathcal{R}_l^{\mathrm{d}}$, in blue). (*Left*): the effective reproduction numbers for the seven nodes corresponding to the provincial aggregation shown in Fig. 2. (*Right*): daily reported data (gray) and the simulated infections as inferred by our SMC method (red). For all plots, solid lines represent the median of the particles' sets and shades represent their 90% C.I. The fractions of mobile individuals for each node, $\xi_l(t)$ (with $l = 1, 7$) and the associated fractions of infections caused by mobility, $\eta_l(t)$ are shown in Fig. 5.

population of the connected communities. The particle filtering approach applied to the disconnected formulation $\mathcal{R}^{\mathrm{d}}(t)$ (which closely approximates the epidemiological golden standard of the computation of the effective reproduction number (8, 9), *SI Appendix*, Fig. S9) may in fact overestimate (or, more rarely, underestimate) the actual value of $\mathcal{R}^{\mathrm{c}}(t)$. Differences emerge when human mobility, subsumed by the connection matrix $\mathbf{C}$ (*SI Appendix*), is responsible for a number of new infections that proves significant compared to the internally generated ones. As lockdown policies were affected by near real-time, unit-exceeding estimates of $\mathcal{R}^{\mathrm{d}}(t)$ from data, attention should be paid to the range of values—often exceeding the unit value threshold—obtained in specific nodes when mobility patterns generate a significant number of infections that are inappropriately attributed to the node (below for a quantification). Fig. 4 summarizes the main differences between the spatially connected and the spatially disconnected effective reproduction number timeseries. While the mean absolute percentage deviation maintains below 10% for six out of seven provinces, we identify a 15% deviation for the province of Rovigo. At the same time, we highlight for three out of seven provinces (Vicenza, Padua, and Rovigo) a fraction of time, where the two timeseries of $\mathcal{R}^{d}(t)$ and $\mathcal{R}^{c}(t)$ lie on opposite sides of the unit threshold, close to, or higher than, 10%.

Locally reported cases synchronize relatively soon after the outbreak, correlating with a relatively uniform seeding of the epidemic in the various provinces and in response to the lockdown imposed after March 2020 (Fig. 2). The results for $\mathcal{R}^{\mathrm{c}}(t)$ and $\mathcal{R}^{\mathrm{d}}(t)$ are often indistinguishable for the most populous provinces, which show large figures of recorded infections (in particular, the province of Verona). Noteworthy instead are the differences between the connected and disconnected reproduction numbers for the province of Rovigo and less significantly for Padua and Vicenza (Fig. 3). Discrepancies are to be ascribed to different origins of the inbound/outbound mobility compared to the resident population responsible for the internal infections. In fact, Fig. 5 shows the coefficients $\xi_l(t)$ of outgoing mobility along with the fraction $\eta_l(t)$ of mobility-induced infections for each province. The outgoing mobility vastly reduces after the onset of the pandemic and then rises back during summer 2020, to decrease afterward during the 2020 to

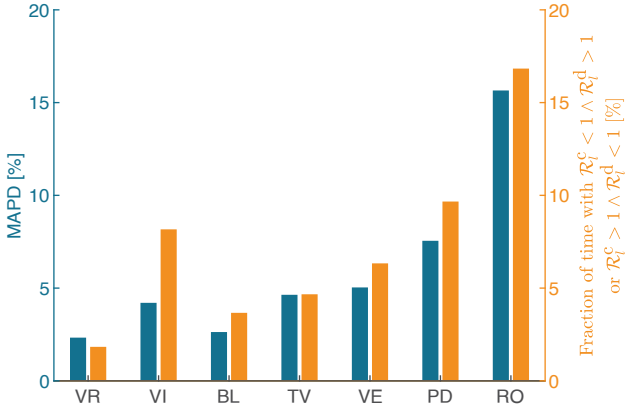

Fig. 4. Blue: mean absolute percentage deviation (MAPD) between the spatially connected and spatially disconnected versions of the effective reproduction number, as displayed in Fig. 3. Orange: percentage fraction of time where the two versions of the effective reproduction number yield values that are opposite in side with respect to the unit value of the reproduction number.

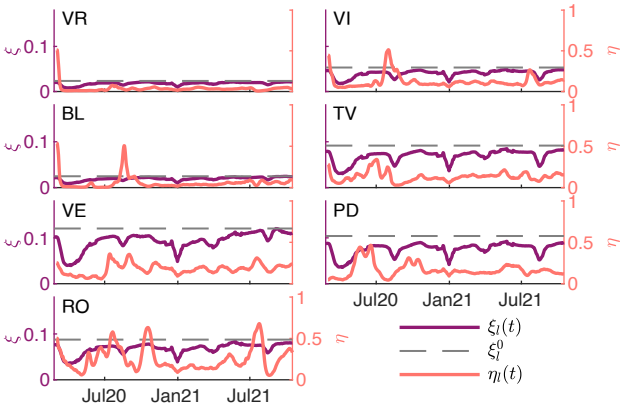

Fig. 5. Outgoing mobility coefficients ξ_l (smoothed timeseries in purple, prepandemic mobility in gray) and fraction of mobility-induced infections $\eta_l(t)$ (orange) for the example shown in Fig. 3. Because the outgoing mobility is estimated by modulating prepandemic levels with Google mobility trends (*SI Appendix*), which are susceptible to weekly fluctuations, we smoothed the data with a 7-d moving average.

2021 winter COVID-19 waves, following containment measures decided by the government. The proportion of mobility-induced infections, in turn, accounts for the quota of infections that are not generated locally (that is, infector and infectee both residents of the same node where the infection occurs). The proportion of outgoing mobility $\xi_l(t)$ for the arbitrary node l (Fig. 5) usually proves lower than the proportion $\eta_l(t)$ of mobility-induced infections, reflecting how infections may not only be imported via resident mobile individuals but also due to contacts with infected individuals belonging to a different community exporting the virus. This is a combined result of mobility and the time-varying values of the effective reproduction number. We observe that, at the beginning of the epidemic, $\eta_l(t)$ decreased drastically during the spring of 2020, when Italy was locked down, to bounce back during the summer and following the introduction of new variants into the territory of Veneto Region. This parameter shows that in many cases, local infections have sparked up because of imported infections from other communities, therefore suggesting that local temporary flare-ups could have seeded infections elsewhere, thus propagating the epidemic. The cases of the provinces of Belluno and Vicenza during the summer of 2020 are interesting in that they display flare-ups of imported cases (Fig. 5). This example highlights another important feature of our method: even if $\mathcal{R}^{\mathrm{d}}(t)$ and $\mathcal{R}^{\mathrm{c}}(t)$ are almost indistinguishable, in fact, the spatial approach allows us to quantify and distinguish the temporal evolution and the origins of the infections.

Discussion

The less populated node, Rovigo, undergoes a substantial net import of infections (Fig. 5), arguably because of commuting. In these cases, $\mathcal{R}^{\mathrm{d}}(t)$ may (Rovigo) or may not (Belluno) overestimate $\mathcal{R}^{\mathrm{c}}(t)$ (Fig. 4). Spatially connected effective reproduction numbers may therefore differ significantly from their spatially disconnected counterparts that are currently used in some cases. Conditions conducive to this result are far from rare. They basically imply marked heterogeneities among the connected human communities also reflected in different population sizes and shares thereof engaging in commuting. These results assume a certain importance because near real-time estimates of $\mathcal{R}^{\mathrm{c}}(t)$ would often not exceed unity as opposed to the related $\mathcal{R}^{\mathrm{d}}(t)$,

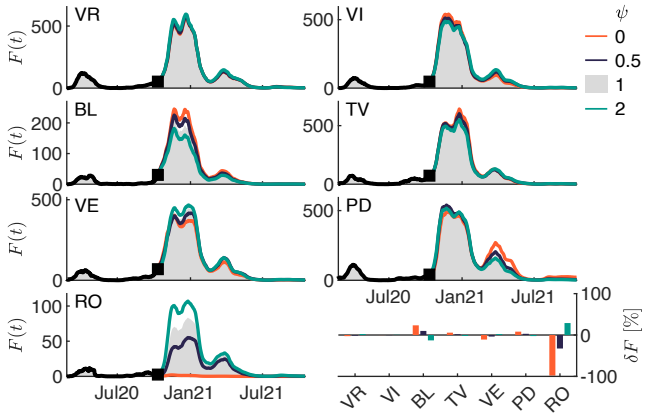

Fig. 6. Daily cases estimated in each province imposing the connected effective reproduction numbers $\mathcal{R}_I^c(t)$ shown in Fig. 3 and different scenarios of mobility, namely no ($\psi = 0$), halved ($\psi = 1/2$), or doubled outgoing mobility ($\psi = 2$). The square in each figure highlights the time of the onset of modified mobility. The shaded area indicates the measured cases in each province. *Lower – Right* plot: for each province, the percentage change in the number of total cases relative to the three mobility scenarios.

which might mislead the interpretation of the actual changes occurring in disease transmission over time.

The significance of spatial effects in the estimation of reproduction numbers is strengthened by the results displayed in Fig. 6, where we show the number of infections that would have occurred if mobility had been altered by a dimensionless factor ψ after a given time (in the example, at the onset of the second wave in October 2020). We note that changes in mobility may enhance or reduce the number of new infections, depending on the nature and the relevance of mobility effects, thus supporting our tenet. Most notable is the nearly complete collapse of estimated infections in the Province of Rovigo in the case of shutdown of all forms of mobility.

Obviously, our approach is not devoid of assumptions. In particular, whatever geographic context one focuses on, some possibly relevant mobility is neglected—even at the continental scale, airborne travel from remote places may be the cause of epidemic seeding within naive populations (14). A geographical limitation of our study is posed by the restriction of the chosen area of interest. In Region Veneto case, all connections to and from neighboring regions are neglected to contain the computational burden. A sensible choice of geographical context would need to be dictated by the relative proportion of internally generated cases facing infection drivers to/from the exterior, usually not known a priori. A different set of assumptions concerns the manner in which possibly different restrictions apply to connected nodes, reflected in the respect of restrictions belonging with the departure or the arrival nodes (*Materials and Methods*). In addition, we assume that the Veneto region adopted a homogeneous swab testing effort across its provinces, which is supported by the fact that healthcare policies in Italy are managed at a regional scale. Also, Veneto is remarkable for its policy requiring a much higher swab testing rate than most other regions in Italy. However, if this were not the case, the results provided by our spatially connected framework would require adjustments to the fundamental Eq. **1** to account for the heterogeneity of the local sampling efforts in different nodes. A generalization of the present framework is certainly worth further investigations in future developments.

The nature of this exercise, which is intended to be a demonstration of the application and relevance of the spatially connected framework at hand, should not be intended as a direct evaluation of the containment measures that were implemented in Italy in 2020 and 2021, due to the nature of our assumptions. We also cannot advocate for any application scale of our framework as it is dependent on an array of factors that falls outside the scope of our work. We stress, however, that this paper highlights the potential importance of the spatially connected framework when computing the effective reproduction number of a pathogen spreading within a metapopulation.

In conclusion, our results suggest that regardless of the computational technique adopted to solve Eq. **1**, challenges arise for planning containment measures guided by detected changes in disease transmission if spatially disconnected reproduction numbers are employed. These are straightforward to compute in near-real time from epidemiological data. Connected reproduction numbers require additional information and are more involved to compute, yet, they better portray the actual origins of the infections and thus give a more accurate view of the unfolding epidemic by including mobility data/proxies that are often publicly available. Practical consequences of particular importance arise when local containment measures are made to depend on estimates of the reproduction number exceeding the unity threshold because they may be influenced by the neglected connectivity.

Materials and Methods

A. Derivation of the Spatially Connected Effective Reproduction Number. The computation of the local (i.e., spatially disconnected) effective reproduction number $\mathcal{R}_I^d(t)$ in isolated nodes I is typically devised on theoretical considerations and specific COVID-19 studies (3, 5, 7, 8, 30). The equation governing the expected new cases, $\hat{F}_I(t)$, at time t based on previous infections is given by Eq. **2**. However, if the community I is not completely isolated, it is reasonable to assume that a quota of the new infections in I might be due to contacts with infectors residing in other communities and thus likely determined by different values of the effective reproduction number. To formalize this concept, we assume that the metapopulation is subdivided into N communities of size n_I ($I = 1, \ldots, N$). Due to local restrictions or different levels of awareness and personal protection, each node is associated with a different (connected) effective reproduction number $\mathcal{R}_I^c(t)$.

In the following, we posit a coupled mechanism of infection where the infector (primary infection) and the infectees (secondary infections) come from two different communities, k and I, respectively, and meet in a third community j possibly different from both. Obviously, two or all of these communities may coincide in particular cases. The number of secondary infections produced by one infector residing in k is estimated by $\mathcal{R}_k^c(t)$. This is motivated by the idea that the infector behaves in accordance to the restrictions and the level of awareness of their own node of origin. The flow of primary infectors residing in k and reaching node j $\left(C_{jk}(t)\int_0^\infty \beta(\tau)F_k(t-\tau)\mathrm{d}\tau\right)$ mixes with a fraction of individuals coming from I $\left(C_{jI}(t)n_I\right)$. The secondary infections generated in j by infectors residing in k are therefore $C_{jk}(t)\mathcal{R}_k^c(t)\int_0^\infty \beta(\tau)F_k(t-\tau)\mathrm{d}\tau$. They occur in individuals of node I proportionally to the quota of individuals of I temporarily present in j, $C_{jI}(t)n_I/\sum_{m=1}^N C_{jm}n_m$. This yields to the formula shown in Eq. **1** and reported below:

$$\hat{F}_I(t) = \sum_{j=1}^{N} \frac{C_{jI}(t)n_I}{\sum_{m=1}^{N} C_{jm}(t)n_m} \sum_{k=1}^{N} C_{jk}(t)\mathcal{R}_k^c(t)\int_0^\infty \beta(\tau)F_k(t-\tau)\mathrm{d}\tau.$$

We illustrate the rationale of this approach in Fig. 7.

In practice, our generalization accounts for the occurrence of three types of infections detected and recorded at an arbitrary node (say I):

- the case of primary and secondary infections occurring in I;
- the case of a secondary infection of a commuting resident of I occurred at any other interconnected node j, for a contact with an infected resident of j or any other infected traveler say, from node k;
- noncommuting residents in I infected by any infected traveler from a node k connected to I.

Another approach to the generalization of Eq. **2** exists and is derived in *SI Appendix, Eq. S4*. We stress that, when mobility is neglected and the connection matrix reduces to the identity matrix, estimates of the new infections reduce to the standard expression shown in Eq. **2** that also features in the popular EpiEstim code (8, 9).

B. Derivation of the Time-Varying Connection Matrix. To represent the daily fluxes of individuals (and thus the possible contacts) among communities, we introduce a connection matrix, $\mathbf{C}$, whose elements C_{jI} represent the fractions of individuals resident in community I that are temporarily present in community j (with $j = I$ being possible and C_{II} representing the fraction of noncommuting individuals). The connection matrix is stochastic, i.e., $\sum_{j=1}^{N} C_{jI} = 1$ for all N nodes ($I = 1, \ldots, N$).

To evaluate the temporal changes of matrix $\mathbf{C}(t)$, we introduce the fraction of mobile individuals in each node, $\xi_I(t)$, defined as,

$$\xi_I(t) = \sum_{j \neq I} C_{jI}(t) = 1 - C_{II}(t), \quad \forall I = 1, \ldots, N.$$

For simplicity, here, we represent the temporal changes in mobility as changes in the fraction of mobile individuals, $\xi_I(t)$, while keeping unchanged the probabilities of reaching their destination. Let us then introduce the prepandemic connection matrix $\mathbf{C}^0$ (i.e., the connection matrix reflecting the conditions that existed before the onset of the COVID-19 outbreak). The proportion of outgoing mobility from node I is therefore

$$\xi_I(t) = \xi_I^0 \psi_I(t),$$

where $\xi_I^0 = 1 - C_{II}^0$ is estimated through the prepandemic connection matrix and $\psi_I(t)$ measures the change in time of outgoing mobility. Because of the property of column-stochasticity, the diagonal term needs to be equal to $C_{II}(t) = 1 - \xi_I(t)\ \forall I$. Given the auxiliary matrix $\mathbf{Q} = (\mathbf{C}^0 - \boldsymbol{I} + \boldsymbol{\xi}^0)(\boldsymbol{\xi}^0)^{-1}$, where $\boldsymbol{I}$ is the identity matrix of size N and $\boldsymbol{\xi}^0$ is a diagonal matrix whose nonnegative terms are the elements ξ_I^0. The time-varying connection matrix $\mathbf{C}(t)$ can then be computed as

$$\mathbf{C}(t) = (\boldsymbol{I} - \boldsymbol{\xi}(t)) + \mathbf{Q}\boldsymbol{\xi}(t),$$

with $\boldsymbol{\xi}(t)$ being a diagonal matrix whose terms are the elements $\xi_I(t)$. The column-stochasticity is preserved.

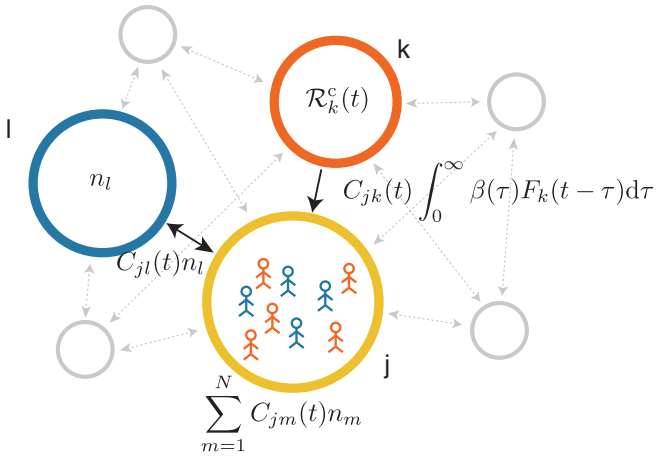

Fig. 7. Rationale of the spatially connected framework described by Eq. **1**. Only three nodes are considered here: the originating node of still uninfected healthy individuals (node I, in blue), the originating node of the fraction of infected individuals (node k, in red), and the node where the infection occurs (node j, in yellow). All nodes serve simultaneously the three purposes.

C. Fraction of Mobility-Induced Infections. We define here another indicator, say η_I, that represents the fraction of infections in node I that are caused by contacts due to mobility. To compute this indicator, we provide an exact solution to an approximate model by considering the incidence $\hat{F}_I^{\mathrm{loc}}(t)$ of local infections, i.e., both infector and infectee residing in node I, with the infection occurring in node I as well. The result (*SI Appendix*) is

$$\frac{1-\eta_I(t)}{(1-\xi_I(t))^2}\frac{\sum_{m=1}^{N} C_{I,m}(t)n_m}{n_I} = \frac{\mathcal{R}_I^c(t)}{\mathcal{R}_I^d(t)}. \quad [3]$$

Eq. **3** links the ratio of the spatially explicit and spatially implicit reproductive numbers to the parameters ξ_I and η_I. It thus provides insight into when and why it is important to consider the connectivity among communities, as well as on whether a given community is a net importer or exporter of infections. The various cases are

- $\mathcal{R}_I^c(t) < \mathcal{R}_I^d(t)$: Community I behaves as a net importer of infections, i.e., the amount of local secondary infections caused by primary infections elsewhere exceeds the secondary infections elsewhere caused by a primary infection in I;
- $\mathcal{R}_I^c(t) > \mathcal{R}_I^d(t)$: Community I behaves as a net exporter of infections, i.e., there are more infections caused in another node $k \neq I$ due to a primary case in I than the other way around;
- $\mathcal{R}_I^c(t) = \mathcal{R}_I^d(t)$: Community I imports as many infection as it exports; or (unrealistic case) it is completely disconnected from other communities.

SI Appendix, Fig. S6 illustrates the comparison of computational results with Eq. **3**.

D. Setup of the Synthetic Example. In the example shown in Fig. 1, the initial connection matrix is defined as

$$\mathbf{C}^0 = \begin{pmatrix} 0.91 & 0.05 & 0.10 \\ 0.05 & 0.83 & 0.05 \\ 0.04 & 0.12 & 0.85 \end{pmatrix}.$$

By assigning a suitable time-varying, sinusoidal mobility pattern (*SI Appendix*, section 5), we obtain elements $C_{jI}(t)$ of the matrix that read:

$$C_{jI}(t) = \frac{C_{jI}^0}{\xi_I^0}\xi_I(t), I \neq j;$$

so that the full matrix becomes (*SI Appendix*)

$$\mathbf{C}(t) = \begin{pmatrix} 1-\xi_1(t) & \frac{0.05}{0.05+0.12}\xi_2(t) & \frac{0.10}{0.10+0.05}\xi_3(t) \\ \frac{0.05}{0.05+0.04}\xi_1(t) & 1-\xi_2(t) & \frac{0.05}{0.10+0.05}\xi_3(t) \\ \frac{0.04}{0.05+0.04}\xi_1(t) & \frac{0.12}{0.05+0.12}\xi_2(t) & 1-\xi_3(t) \end{pmatrix}.$$

By design, we wanted the population size of the three nodes to be heterogeneous: We used 80,000, 450,000, and 700,000 inhabitants, respectively. The true values of the effective reproduction number for the three nodes that are used to generate fictitious case reports also follow a seasonal pattern (*SI Appendix*). Those for the first and second nodes are defined in a sinusoidal manner (*SI Appendix* and Fig. 1). The effective reproduction number for node 3 is chosen arbitrarily from the repository https://github.com/covid-19-Re/dailyRe-Data and its values are multiplied by a factor 1.05 for convenience.

E. Setup of the Application to the Epidemic in Region Veneto. Incidence and mobility data have been collected at the provincial level (second tier administrative division in Italy). We choose to run our analyses on this granularity because we estimated that the finer one, municipalities (Fig. 2), would be inappropriate for a credible inference of the effective reproduction number. In fact, many municipalities reported new cases only sporadically, thus preventing a meaningful estimation of the effective reproduction numbers, especially when the disconnected method is implemented (8). In Region Veneto, there are seven nodes at the second level division: the provinces of Verona, Vicenza, Belluno, Treviso, Padua, Rovigo, and the Metropolitan City of Venice. Data available at finer granularity are properly aggregated.

Epidemiological data. In the second experiment on the Italian COVID-19 epidemic, we considered the daily SARS-CoV-2 infections reported by the Italian Civil Protection Department available from https://github.com/pcm-dpc/COVID-19 at a provincial level to date. To prevent issues arising from inhomogeneous daily testing efforts, namely due to fewer swab tests taking place during weekends, we apply a 14-d moving average to the data. The data in input to the proposed algorithm are consequently artificially smoothed by a widely accepted procedure for curated data (https://www.epicentro.iss.it/coronavirus/sars-cov-2-sorveglianza-dati).

Generation of the connection matrix. The connection matrix between provinces is assigned on the basis of commuting data provided by the Italian Institute of Statistics (ISTAT) (accessible at: https://www.istat.it/it/archivio/139381) that reports the number of individuals commuting between two different nodes for work or study reasons. To limit our selection to the mobility fluxes happening within the region of Veneto, we select the submatrix corresponding to the seven nodes at the second administrative level within the region. We further proceed to normalize the matrix by the reported mobile population of the corresponding node so that the resulting matrix $\mathbf{C}^0$ is column-stochastic, i.e., the column-wise sums are all equal to 1. This choice takes into account the fact that in the reported commuting population (which on average, in Region Veneto, is 45 to 55% of the actual resident population) only mobility to the workplace or school is taken into account, while leisure mobility is neglected. The resulting entries, C^0_{jl}, represent the daily fraction of mobile individuals originating in node l that reach j as their destination node. Because our work only considers the provinces of Region Veneto, we disregard connections to and from nodes that are not part of it. Matrix $\mathbf{C}^0$ is shown in *SI Appendix*, Fig. S3 (*SI Appendix*). The population resident in the Veneto's provinces is also obtained through the Italian Institute of Statistics (accessible at http://dati.istat.it/Index.aspx?QueryId=18549).

Finally, to describe the changes in the mobility patterns during the course of the pandemic, portrayed by the function $\psi_l(t)$, we modified the fraction of mobile individuals in each province in accordance with the changes of "Workplace mobility" provided by Google's Community Mobility reports (https://www.google.com/covid19/mobility/).

F. Distribution of the Generation Times. In this example, we assume gamma-distributed with a mean of 5.20 d and a SD of 1.72 d (31). This mean generation time is only slightly lower than estimates computed upon the first COVID-19 wave in the neighboring Region Lombardy (17, 23). In the convolution integral of Eq. **1**, we evaluate this probability distribution function up to a cutoff upper bound of 21 d, past which we assume $\beta(\tau > 21 \text{ days}) = 0$.

G. Inference through a Sequential Monte Carlo Method. Our procedure involves a sequential Monte Carlo method (SMC), also known as particle filter, to infer the nodal effective reproduction numbers. We assume that the normalized incidence (ratio of new cases to the local population) recorded on day t in node l is affected by a lognormal noise (model error), that is $I_l(t) = \hat{I}_l(t)\varepsilon_l(t)$, with $\ln(\varepsilon_l(t))$ being normally distributed with mean equal to zero and unknown variance σ_l^2. We assume statistical independence among the errors occurred in different instants and different nodes. These assumptions allow us to define the likelihood function that is implemented in the algorithm. By recalling Eq. **1**, we consider the estimated incidence as a function of the effective reproduction numbers at all nodes: $\hat{I}_l(t) = f_l(t, \boldsymbol{\mathcal{R}}(t), \boldsymbol{\theta})$, where $\boldsymbol{\mathcal{R}}(t)$ is a vector containing the values at time t of the nodal effective reproduction numbers and $\boldsymbol{\theta}$ is a vector of unknown parameters. Let also $\mathbf{I}(t)$ be the vector containing the values of the nodal $I_l(t)$. The following relationship holds:

$$\ln\left(\frac{I_l(t)}{f_l(t, \boldsymbol{\mathcal{R}}(t), \boldsymbol{\theta})}\right) = \ln\left(\varepsilon_l(t)\right). \quad [4]$$

The assumption of independent errors among nodes allows us to write the likelihood function of the recorded incidences on all nodes $l = 1, \ldots, N$ given the values of effective reproduction numbers as:

$$\mathcal{L}(\mathbf{I}(t), \boldsymbol{\mathcal{R}}(t)) = \prod_{l=1}^{N} \frac{1}{\sqrt{2\pi\sigma_l^2 I_l(t)}} \exp\left(-\frac{1}{2\sigma_l^2}\left[\ln\left(\frac{I_l(t)}{f_l(t, \boldsymbol{\mathcal{R}}(t), \boldsymbol{\theta})}\right)\right]^2\right). \quad [5]$$

We address the above problem through the implementation of a specific particle filter (SMC) (24, 26, 27). We assume that, at each day t, the probability distribution of the nodal effective reproduction numbers, $\boldsymbol{\mathcal{R}}(t) = \{\mathcal{R}_l^c(t)\}_{l=1}^N$, is described by the empirical weighted distribution of N_p realizations, $(\boldsymbol{\mathcal{R}}^{(i)}(t), w_t^{(i)})$, where $w_t^{(i)}$ is the weight representing the importance of the i-th particle in the distribution at time t. We refer the reader to (*SI Appendix*) for additional details regarding the implementation of the particle filter.

Data, Materials, and Software Availability. All data and all implemented code are archived at the following Zenodo repository: https://doi.org/10.5281/zenodo.7869249 and are also available at the following GitHub repository: https://github.com/COVID-19-routes/Spatially-Connected-Rt (32).

ACKNOWLEDGMENTS. C.T. and A.R. acknowledge funding from the Swiss NSF via the project "Optimal control of intervention strategies for waterborne disease epidemics" (200021-172578). E.B., D.P., and A.R. acknowledge funding from Fondazione Cassa di Risparmio di Padova e Rovigo (IT) through its grant 55722. D.P. acknowledges funding from the Ca' Foscari University of Venice ("Fondi di primo insediamento"). D.P., E.B., L.M., and R.C. acknowledge funding from the Italian Ministry of University and Research through the project EPIDOC (Epidemiological Data assimilation and Optimal Control for short-term forecasting and emergency management of COVID-19 in Italy), FISR-2020IP-04249. The authors wish to thank Giorgio Corani and Mario Zanon for useful discussions.

Author affiliations: [a]Laboratory of Ecohydrology, École Polytechnique Fédérale de Lausanne, Lausanne 1015, Switzerland; [b]Dipartimento di Scienze Ambientali, Informatica e Statistica, Università Ca' Foscari Venezia, Venezia 30172, Italy; [c]Dipartimento di Elettronica, Informazione e Bioingegneria, Politecnico di Milano, Milano 20133, Italy; [d]Dipartimento di Meccanica, Politecnico di Milano, Milano 20133, Italy; and [e]Dipartimento di Ingegneria Civile, Edile e Ambientale (ICEA), Università di Padova, Padova 35131, Italy

1. R. M. Anderson, R. M. May, Population biology of infectious diseases: Part i. *Nature* **280**, 361–367 (1979).
2. R. M. Anderson, R. M. May, *Infectious Diseases of Humans. Dynamics and Control*. (Oxford University Press, 2008).
3. J. Wallinga, P. Teunis, Different epidemic curves for severe acute respiratory syndrome reveal similar impacts of control measures. *Am. J. Epidemiol.* **160**, 509–516 (2004).
4. M. Lipsitch *et al.*, Transmission dynamics and control of severe acute respiratory syndrome. *Science* **300**, 1966–1970 (2003).
5. J. Wallinga, M. Lipsitch, How generation intervals shape the relationship between growth rates and reproductive numbers. *Proc. R. Soc. B* **274**, 599–604 (2007).
6. G. Scalia Tomba, A. Svensson, T. Asikainen, J. Giesecke, Some model based considerations on observing generation times for communicable diseases. *Math. Biosci.* **223**, 24–31 (2010).
7. T. Britton, G. Scalia Tomba, Estimation in emerging epidemics: Biases and remedies. *J. R. Soc. Interface* **16**, 20180670 (2019).
8. A. Cori, N. M. Ferguson, C. Fraser, S. Cauchemez, A new framework and software to estimate time-varying reproduction numbers during epidemics. *Am. J. Epidemiol.* **178**, 1505–1512 (2013).
9. K. Gostic *et al.*, Practical considerations for measuring the effective reproductive number, R_t. *PLoS Comput. Biol.* **16**, e1008409. (2020).
10. G. Guzzetta *et al.*, Potential short-term outcome of an uncontrolled COVID-19 epidemic in Lombardy, Italy, February to March 2020. *Euro Surveill.* **25**, 2000293 (2020).

11. O. Diekmann, H. Hesterbeek, T. Britton, *Mathematical Tools for Understanding Infectious Disease Dynamics* (Princeton University Press, 2013).
12. C. Zhan, C. K. Tse, Y. Fu, Z. Lai, H. Zhang, Modeling and prediction of the 2019 coronavirus disease spreading in China incorporating human migration data. *PloS One* **15**, e0241171. (2020).
13. J. T. Wu, K. Leung, G. M. Leung, Nowcasting and forecasting the potential domestic and international spread of the 2019-ncov outbreak originating in Wuhan, China: A modelling study. *Lancet* **395**, 689–697 (2020).
14. M. Chinazzi *et al*., The effect of travel restrictions on the spread of the 2019 novel coronavirus (COVID-19) outbreak. *Science* **368**, 395–400 (2020).
15. M. Gatto *et al*., Spread and dynamics of the COVID-19 epidemic in Italy: Effects of emergency containment measures. *Proc. Natl. Acad. Sci. U.S.A.* **117**, 10484–10491 (2020).
16. E. Bertuzzo , et al., The geography of COVID-19 spread in Italy and implications for the relaxation of confinement measures. *Nat. Commun.* **11**, 1–12 (2020).
17. V. Marziano *et al*., Retrospective analysis of the Italian exit strategy from COVID-19 lockdown. *Proc. Natl. Acad. Sci. U.S.A.* **118** (2021).
18. Q. Liu *et al*., Measurability of the epidemic reproduction number in data-driven contact networks. *Proc. Natl. Acad. Sci. U.S.A.* **115**, 12680–12685 (2018).
19. L. Mari *et al*., The epidemicity index of recurrent SARS-CoV-2 infections. *Nat. Commun.* **12**, 2752 (2021).
20. B. Cazelles, C. Champagne, J. Dureau, Accounting for non-stationarity in epidemiology by embedding time-varying parameters in stochastic models. *PLoS Comput. Biol.* **14**, e1006211 (2018).
21. J. C. Lemaitre, J. Perez-Saez, A. S. Azman, A. Rinaldo, J. Fellay, Assessing the impact of non-pharmaceutical interventions on SARS-CoV-2 transmission in Switzerland. *Swiss Med. Wkly* **150**, w20295 (2020).
22. D. Pasetto, J. Lemaitre, E. Bertuzzo, M. Gatto, A. Rinaldo, Range of reproduction number estimates for COVID-19 spread. *Biochem. Biophys. Res. Commun.* **538**, 253–258 (2021).
23. D. Cereda *et al*., The early phase of the COVID-19 outbreak in Lombardy Italy. *Epidemics* **37**, 100528. (2021).
24. A. A. King, D. Nguyen, E. L. Ionides, Statistical inference for partially observed Markov processes via the R package POMP. *J. Stat. Softw.* **69**, 1–43 (2016).
25. S. Shrestha, A. A. King, P. Rohani, Statistical inference for multi-pathogen systems. *PLoS Comput. Biol.* **7**, e1002135. (2011).
26. D. Pasetto, F. Finger, A. Rinaldo, E. Bertuzzo, Real-time projections of cholera outbreaks through data assimilation and rainfall forecasting. *Adv. Water Resour.* **108**, 345–356 (2017).
27. D. Pasetto *et al*., Near real-time forecasting for cholera decision making in Haiti after hurricane Matthew. *PLoS Comput. Biol.* **14**, e1006127. (2018).
28. M. Manica *et al*., Intrinsic generation time of the SARS-CoV-2 Omicron variant: An observational study of household transmission. *Lancet Reg. Health Eur.* **19**, 100446. (2022).
29. D. Kim *et al*., Estimation of serial interval and reproduction number to quantify the transmissibility of SARS-CoV-2 Omicron variant in South Korea. *Viruses* **14**, 533 (2022).
30. J. A. Backer, D. Klinkenberg, J. Wallinga, Incubation period of 2019 novel coronavirus (2019-nCoV) infections among travellers from Wuhan, China. *Euro Surveill.* **25**, 2000062 (2020).
31. T. Ganyani *et al*., Estimating the generation interval for coronavirus disease (COVID-19) based on symptom onset data, March 2020. *Euro Surveill.* **25**, 2000257 (2020).
32. C. Trevisin *et al*., Spatially explicit effective reproduction numbers from incidence and mobility data. Zenodo. Deposited 26 April 2023.